Int. J. Appl. Comput. Math (2026) 12:25
https://doi.org/10.1007/s40819-026-02100-2

ORIGINAL PAPER

Turing Bifurcations on Elliptical Domains: A Deviation from Rectangular and Circular Limits

Thomas E. Woolley[1]

Received: 24 November 2025 / Accepted: 6 February 2026

Abstract
Turing patterns have been extensively studied on simple geometries such as lines, squares, rectangles, and circles. Consequently, many biological and physical applications of Turing's theory approximate their domains to have simple geometries. In particular, thin domains are often approximated as one-dimensional lines or rectangles, whereas the actual geometry may be curved and closer to a stretched ellipse. Thus, we investigate Turing patterns on ellipses and show that they exhibit two distinct limiting behaviours: (i) they tend to those on the circular domain as the ellipse's aspect ratio approaches unity; (ii) they do not converge to the behaviour of a one-dimensional line as the ellipse becomes thin. This contrasts with rectangular domains, where the bifurcation structure smoothly tends to that of a one-dimensional line as the rectangle's height is reduced. Using a combination of analytical methods involving Mathieu equations and numerical bifurcation tracking, we demonstrate that the bifurcation modes in an elliptical domain are intrinsically coupled in both radial and angular directions, preventing simple interpolation between circular and linear limits. The results provide insights into the role of domain geometry in governing Turing instabilities and pattern selection, highlighting the distinctive behaviour of ellipses compared to other commonly studied geometries.

Keywords Turing patterns · Reaction-diffusion systems · Elliptical domains · Mathieu equations · Bifurcation analysis · Domain geometry

Introduction

Turing patterns [1] mechanistically describe the production of spatially periodic structures from the destabilisation of a homogeneous state, due to the interplay of reaction and diffusion processes. These patterns provide a mechanism for understanding a variety of natural phenomena, including animal coat markings, cellular organisation, and chemical reactions [2]. The mathematical foundations of Turing patterns have been widely studied in reaction–diffusion systems. In such systems, small perturbations of an initially uniform state can grow into stable spatial structures when conditions on diffusion rates and reaction kinetics are satisfied [3]. Critically, the emergence and stability of these patterns depend not only on the

✉ Thomas E. Woolley
woolleyt1@cardiff.ac.uk

[1] Cardiff School of Mathematics Cardiff University, Senghennydd Road, Cardiff CF24 4AG, UK

reaction terms but also on the geometry and boundary conditions of the domain in which they occur [4, 5].

It is well known that the appearance of Turing patterns depends on the size of the domain on which they are simulated [3]. Namely, the domain must be larger than a critical size for a pattern to emerge [6]. In this work, we will be using the horizontal width of our domains as a bifurcation parameter and referring to the width at which the homogeneous steady state destabilises as the critical length.

Notably, the two-dimensional Turing analysis of the rectangle reveals that the initial patterning bifurcation arises from a superposition of perpendicular one-dimensional patterns [7, 8]. Consequently, the critical length of a rectangle is equivalent to that of a one-dimensional line, meaning that a rectangle can be arbitrarily thin in the vertical direction without influencing its critical horizontal length. This aligns with classical predictions of separable eigenmode solutions in rectangular domains [3]. Such results can be compared to derivations involving circular domains, where it has been observed that the critical length, or radius, is larger than that of a square domain [4].

In applications, complicated curved domains are often simplified to squares and rectangles [9]. Moreover thin domains are frequently modelled by reducing a two-dimensional problem to one dimension [10]. Such simplifications and dimensional reductions implicitly assume that the instability threshold and leading unstable modes are governed only by the longest length scale, so that curvature and transverse structure can be ignored. We aim to test how far such simplifications can be trusted.

Since the vertical and horizontal scales of an ellipse can be independently varied (similar to a rectangle), we may hypothesise that an arbitrarily thin ellipse would behave similarly to a thin rectangle. However, we show that this is not the case. Moreover, one might expect the relationship between the critical length and vertical height of an ellipse to interpolate smoothly between the flat line and the circle. Although the bifurcation structure tends to that of the circle as the aspect ratio approaches one, it does not converge to the one-dimensional limit as the ellipse becomes thin.

The results we aim to understand are illustrated in Fig. 1, where a Turing system (see equations (21) and (22)) is simulated on circular, thin rectangular, and thin elliptical domains (top to bottom, respectively) with increasing horizontal widths, left to right. For small widths we observe that no pattern forms on any domain. As the width increases, the pattern appears first on the thin rectangle, then on the circle, and finally on the ellipse.

These findings have implications for biological morphogenesis, where tissue and organ structures often approximate elongated domains rather than idealised geometric shapes [11].

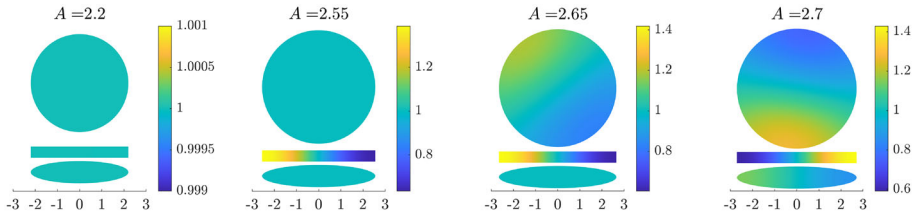

Fig. 1 A simulation of equations (21) and (22) on three domains. In each column, the top domain is a circle, the middle domain is a rectangle, and the bottom domain is an ellipse. The horizontal width of each domain is $[-A, A]$ and increases left to right, with A denoted above each figure. Only the concentration variable ϕ is visualised in each case. The ψ variable would provide a similar, but out of phase pattern. The heights of the rectangle and the semi-major axis length of the ellipse are both $1/2$

Equally, our bifurcation results can be applied to material science, where reaction-diffusion mechanisms govern the self-assembly of nanostructures [12]. Equally, in the development of synthetic materials, it is crucial to understand how shape influences pattern since specific patterning properties are being designed [13].

In this paper we use radial and angular Mathieu equations to characterise how the critical length depends on the ellipse aspect ratio. This reveals why elliptical domains are fundamentally different from circular and rectangular domains from the point of view of a Turing bifurcation. These analytical results are then supported by simulations and numerical continuation of the bifurcation structure.

Geometry

Before we define the reaction-diffusion framework which will produce the Turing patterns we first define the elliptical domain and coordinate system used in our analysis. We define a domain $\Omega \in \mathbb{R}^2$ to be the interior of the ellipse with foci at $(-a, 0)$ and $(a, 0)$ defined by $\Omega = \{(x, y)|x = a\cosh(u)\cos(v), y = a\sinh(u)\sin(v) \text{ where } u \in [0, u_c), v \in [0, 2\pi)\}$ [14, 15]. The boundary is then given by $\partial\Omega = \{(x, y)|x = a\cosh(u_c)\cos(v), y = a\sinh(u_c)\sin(v) \text{ where } v \in [0, 2\pi)\}$. The length of the u interval, u_c, and the foci position, a, will be defined by the lengths of the semi-major axis length, A and the semi-minor axis length, B (see Fig. 2). Explicitly, we assume $A \geq B$ and, thus,

$$a = \sqrt{A^2 - B^2}, \tag{1}$$

$$\tanh(u_c) = \frac{B}{A}. \tag{2}$$

This choice of elliptic coordinates means that the unit directions, $\hat{\boldsymbol{u}}$ and $\hat{\boldsymbol{v}}$, are orthogonal and, for fixed $u \in [0, u_c]$, the $(x(v), y(v))$ curves parametrically describe ellipses with the same foci but the eccentricity decreases from 1 (the one-dimensional line of length 2a) to $\sqrt{1 - B^2/A^2}$. Equally, for fixed v, $(x(u), y(u))$ curves parametrically describe hyperbolae [16].

Through taking different limits of the aspect ratio, the ellipse is able to geometrically interpolate between the one-dimensional line ($B \to 0$) and the circle ($B \to A$). Thus, we will be comparing the elliptic geometry with the circle, radius A, and the one-dimensional line of length $[-A, A]$. Through these definitions we will be using the horizontal half widths of the domains, A, as a means of comparing the domains.

Instability Theory

Let $\phi(\boldsymbol{x}, t)$ and $\psi(\boldsymbol{x}, t)$ be two interacting morphogen populations that exist for all $\boldsymbol{x} \in \Omega$ and for all time $t > 0$. The evolution of ϕ and ψ is defined by interaction equations f and g combined with spatial diffusion at rates D_ϕ and D_ψ, respectively, through the partial differential equations (PDEs)

$$\frac{\partial\phi}{\partial t} = D_\phi\nabla^2\phi + f(\phi, \psi), \tag{3}$$

$$\frac{\partial\psi}{\partial t} = D_\psi\nabla^2\psi + g(\phi, \psi), \tag{4}$$

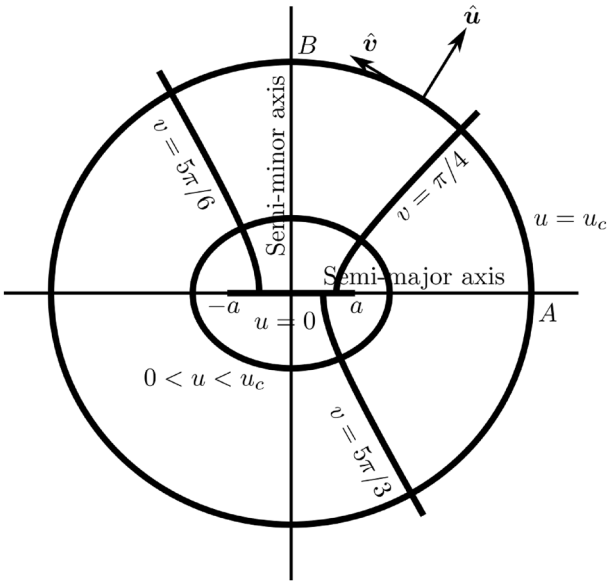

Fig. 2 Schematic diagram of an ellipse relating the Cartesian coordinates and the elliptical coordinates through $(x, y) = (a\cosh(u)\cos(v), a\sinh(u)\sin(v))$, where a is a positive constant, $u \in [0, u_c]$ and $v \in [0, 2\pi]$

where ∇^2 is the Laplacian on Ω. Under the coordinate transformation defined in Sect. 2 the Laplacian is [16, 17]

$$\nabla^2 = \frac{\partial^2}{\partial x^2} + \frac{\partial^2}{\partial y^2} = \frac{2}{a^2(\cosh(2u) - \cos(2v))}\left(\frac{\partial^2}{\partial u^2} + \frac{\partial^2}{\partial v^2}\right). \tag{5}$$

Additionally, we assume that Ω has reflective, or zero-flux boundary conditions, which, due to the definition of the coordinate system, have the simple form

$$\frac{\partial \phi}{\partial u} = 0 = \frac{\partial \psi}{\partial u} \text{ on } \partial\Omega. \tag{6}$$

To finalise the system's description we need to provide an initial condition. By definition a PDE system has a Turing instability if there is a uniform spatial steady state that is stable in the absence of diffusion, which can be driven unstable by the inclusion of diffusion. Defining the spatially uniform state to be (ϕ_s, ψ_s) means we can define the initial condition to be a small random perturbation about this point,

$$(\phi(\boldsymbol{x}, 0), \psi(\boldsymbol{x}, 0)) = \left|(\phi_s, \psi_s) + \left(\eta_\phi(\boldsymbol{x}), \eta_\psi(\boldsymbol{x})\right)\right|, \tag{7}$$

where $\eta_\phi(\boldsymbol{x})$ and $\eta_\psi(\boldsymbol{x})$ are samples drawn from a uniform random distribution on the interval $[-0.1, 0.1]$. The absolute value is to ensure that the initial condition is never negative.

Linear Analysis

Assuming that we can turn the Laplacian into a linear functional [18, 19],

$$\nabla^2 h = -k^2 h, \tag{8}$$

for some function, h, and some values, k, under the given boundary and initial conditions, then we can use standard linear analysis to derive the Turing inequalities that must be satisfied to ensure a Turing instability [3, 20, 21],

$$f_\phi + g_\psi < 0, \tag{9}$$
$$f_\phi g_\psi - f_\psi g_\phi > 0, \tag{10}$$
$$D_\psi f_\phi + D_\phi g_\psi > 0, \tag{11}$$
$$\left(D_\psi f_\phi + D_\phi g_\psi\right)^2 - 4D_\phi D_\psi \left(f_\phi g_\psi - g_\phi f_\psi\right) > 0, \tag{12}$$
$$k_-^2 < k^2 < k_+^2 \text{ where}$$
$$k_\pm^2 = \frac{D_\psi f_\phi + D_\phi g_\psi \pm \sqrt{\left(D_\psi f_\phi + D_\phi g_\psi\right)^2 - 4D_\phi D_\psi \left(f_\phi g_\psi - g_\phi f_\psi\right)}}{2D_\phi D_\psi}, \tag{13}$$

where the subscripts on the f and g functions represent partial derivatives with respect to the subscript and all of the derivatives are evaluated at the homogeneous steady state. Inequalities (9)–(12) are conditions that purely concern the values of the reaction and diffusion components and are independent of the domain. The inequalities ensure that the steady state is stable in the absence of diffusion and that diffusion can drive the steady state to instability, as required.

Inequality (13) links the population's kinetics and diffusion values to the domain's properties through k. Essentially, inequality (13) ensures that the space is big enough to allow a pattern to form. Theoretically, making a domain large enough is usually not a huge restriction on the ability for Turing patterns to form, as we can always ensure to simulate large domains, however inequality (13) allows us to derive the critical horizontal length, A_c (or equivalently u_c), at which the Turing bifurcation occurs. More specifically, we will define A_{circle} and A_{line} to be the critical widths of the circle and line, respectively. Additionally, we will define $A_{\text{ellipse}}(B)$ to be the critical width of the ellipse, where the dependence of A_c on B is highlighted. Since we are considering A to be the bifurcation parameter and increasing the domain size is equivalent to reducing k then the Turing bifurcation will happen when the first nonzero eigenvalue is $k = k_+$.

Eigenvalues of the Laplacian on an Ellipse

Solving equation (8) on elliptical domains has a long history [15, 22], going back to 1868 with work on vibrations of elastic membranes by Mathieu [23]. We approach solving equation (8) by looking for a separable solution of the form $h(u, v) = h_r(u)h_a(v)$, where h_r and h_a are termed the radial and angular components, respectively, as u and v act like radial and angular coordinates (see Fig. 2). Substituting this solution form into equation (8) we derive that h_r and h_a must satisfy

$$h_a'' + (p - 2q\cos(2v))\, h_a = 0, \tag{14}$$
$$h_r'' - (p - 2q\cosh(2u))\, h_r = 0, \tag{15}$$

where $2q = k^2a^2/2$ and p is a coupling constant to be defined. Additionally, we have the constraints that h_a is periodic, with period 2π and

$$\left.\frac{\mathrm{d}h_r}{\mathrm{d}u}\right|_{u_c} = 0. \tag{16}$$

Equations (14) and (15) are known as the angular and radial (or modified) Mathieu equations, respectively. Periodic solutions to equation (14) exist for an infinite set of values of p. These values are separated into two families, p_{cn} and p_{sn}, and indexed by the positive integers, $n = 1, 2, \ldots$. The corresponding two families of 'Mathieu functions of the first kind' are denoted $ce_n(x, q)$ and $se_n(x, q)$ [24], which are sometimes referred to as cosine-elliptic and sine-elliptic, respectively.

Solutions of Eq. (15) can be related to the solutions of Eq. (14) by mapping $x \to \pm Ix$, where I is the imaginary unit. Thus, the solutions of Eq. (15) are denoted $Ce_n(x, q)$ and $Se_n(x, q)$, where [25]

$$Ce_n(x, q) = ce_n(Ix, q), \tag{17}$$

$$Se_n(x, q) = -Ise_n(Ix, q). \tag{18}$$

In addition to periodicity of h_a we also impose the physical assumptions that h and its u derivative are continuous across the $u = 0$ line (see Fig. 2). These restrict the possible forms of h to be either $Ce_n(u, q)ce_n(v, q)$, or $Se_n(u, q)se_n(v, q)$ [24].

Satisfying Eq. (16) requires us to define u_c and, thus, define the critical length of the ellipse at which the Turing patterning bifurcation can occur. Rewriting equation (16) in terms of A and B we have to satisfy

$$\begin{aligned} \frac{\mathrm{d}Ce_n}{\mathrm{d}u}\left(\operatorname{arctanh}\left(\frac{B}{A}\right), k_+^2\left(A^2 - B^2\right)/4\right) = 0, \text{ or} \\ \frac{\mathrm{d}Se_n}{\mathrm{d}u}\left(\operatorname{arctanh}\left(\frac{B}{A}\right), k_+^2\left(A^2 - B^2\right)/4\right) = 0. \end{aligned} \tag{19}$$

For general A and B this must be solved numerically, which will be done in the next section. However, there are two limits that we are interested in; $B \to 0$ and $B \to A$.

For $B \to 0$ we might expect that system would begin to act like the solution on a one-dimensional domain. Deriving the bifurcation conditions on a one-dimensional domain is very common [26, 27] and it is known [4] that the critical length of the line satisfies $k_+ = \pi/(2A_{\text{line}})$ ($2A_{\text{line}}$ being the length of the line), or $k_+ A_{\text{line}} = \pi/2 \approx 1.57$. By doing a series expansion of $\mathrm{d}Ce_n/\,\mathrm{d}u$ about $B = 0$ we find that the derivative is zero when

$$\frac{\left(k_+ A_{\text{ellipse}}(0)\right)^2}{2} = p_{c1}\left(\frac{\left(k_+ A_{\text{ellipse}}(0)\right)^2}{4}\right), \tag{20}$$

where $p_{c1}(q)$ is the characteristic value for $ce_1(x, q)$ [28]. The smallest value satisfying equation (20) can be found numerically to be $k_+ A_{\text{ellipse}}(0) \approx 1.89$, which is bigger than the values for the one dimensional domain. Since k_+ depends only on kinetic and diffusion parameters, which would be the same on both domains, this means that the critical horizontal width of a thin ellipse, $A_{\text{ellipse}}(0)$, does not converge to the one-dimensional line limit A_{line}.

For $B \to A$, we might expect the system would begin to act like the solution on a circular domain. For a circular domain the critical horizontal width (or radius), has to satisfy $B_1'(k_+ A_{\text{circle}}) = 0$, where $B_n(x)$ is the Bessel function of the first kind, order n. The numerical solution of which is known to be $k_+ A_{\text{circle}} \approx 1.84$ [4]. Following the techniques shown in [29] equation (15) can be converted into a modified Bessel's equations, which converges to a standard Bessel equations as $q = k^2(A^2 - B^2)/4 \to 0$, with $a\cosh(u_c) = \sqrt{A^2 - B^2}\cosh(\operatorname{arctanh}(B/A)) \to A$ and $a\sinh(u_c) = \sqrt{A^2 - B^2}\sinh(\operatorname{arctanh}(B/A)) \to A$. Thus, the solution to the elliptical problem tends to the solution of the circular domain as $B \to A$, as expected.

Investigating $A_{\text{ellipse}}(B)$ beyond these two limits is difficult. In the next section we turn to simulation to illustrate that the critical widths on the three domains satisfy $A_{\text{line}} < A_{\text{circle}} \leq A_{\text{ellipse}}(B)$ for all B (producing the result seen in Fig. 1). Thus, although the bifurcation structure on the ellipse may tend to that of a circle, the elliptical domain cannot be thought to act as a means of interpolating between the line and circle, in terms of Turing patterns.

Results

To demonstrate our results we will be using a specific form of the Schnakenberg kinetics [30]

$$\frac{\partial \phi}{\partial t} = \nabla^2 \phi + \frac{1}{10} - \phi + \phi^2 \psi, \tag{21}$$

$$\frac{\partial \psi}{\partial t} = 10\nabla^2 \psi + \frac{9}{10} - \phi^2 \psi, \tag{22}$$

with zero-flux boundary conditions. Substituting these kinetics and parameter values into inequality (13) we find that $k_+^2 = 1/2$ and, thus, $A_{\text{line}} \approx 2.22$ and $A_{\text{circle}} \approx 2.60$.

Figure 3a illustrates the values of the derivatives of the sine- and cosine-elliptic functions, with the zero values being highlighted as black lines. These lines define $A_{\text{ellipse}}(B)$ and we observe that the smallest values of A are given when we set $n = 1$ in the cosine-elliptic function. The $n = 1$ cosine-elliptic solutions correspond to solutions that vary along the major axis of the ellipse (see Fig. 3b), whereas the sine-elliptic solutions correspond to solutions that vary along the minor axis (see Fig. 3c). As A and B become larger (with $A > B$), we see that there would be many overlapping solution regions between the two elliptical solutions and for multiple values of n demonstrating the common occurrence in Turing systems that the patterns become more complex as the two-dimensional space grows.

Note that all the solutions of $\mathrm{d}Se_n/\,\mathrm{d}u = 0$ are approximately parallel to the A-axis, meaning that the existence of solutions is very sensitive to changes in B. This contrasts with the solutions to $\mathrm{d}Ce_n/\,\mathrm{d}u = 0$, where we observe that there is a solution for all $0 < B < A_{\text{circle}}$. Thus, for a fixed B, as we increase the size of the major axis, the pattern will tend to find solutions defined by $\mathrm{d}Ce_n/\,\mathrm{d}u = 0$ because they are the first to appear for all B. Meaning that for long, thin ellipses, $B \ll A$, the solutions would look like Fig. 3b, where stripes would align parallel to the minor axis and vary along the major axis, similar to long, thin rectangles (this is confirmed in Fig. 1).

Figure 4a shows a magnified region of $\mathrm{d}Ce_1/\,\mathrm{d}u = 0$, where we compare the critical patterning radius of the circle (circle marker at (2.60, 2.60)) and critical length of the one-dimensional line (square marker at (2.22, 0)) with the critical widths of the ellipse (thick black line). Figure 4a evidences the results of Sect. 3.2 that $A_{\text{ellipse}}(B) \to A_{\text{circle}}$ as $B \to A_{\text{circle}}$ and that $A_{\text{square}} < A_{\text{ellipse}}(0)$. Moreover, we see that $A_{\text{circle}} < A_{\text{ellipse}}(B)$ for all B. Thus, an elliptical domain cannot be considered to act as a means interpolating patterning dynamics between the one-dimensional line and the circle.

We further confirm the theoretical solutions using `pde2path`, a numerical continuation software package that allows us to derive and track bifurcation structures of PDE systems [31, 32]. Specifically, with zero-flux boundary conditions, the steady state values of (ϕ, ψ) of equations (21) and (22) undergo a supercritical pitchfork Turing bifurcation as the solution domain gets larger. For domains smaller than the critical length the homogeneous steady state is stable. As the domain gets larger the homogeneous solution destabilises and the heterogeneous pattern solution stabilises. The maximum and minimum of the stable solutions

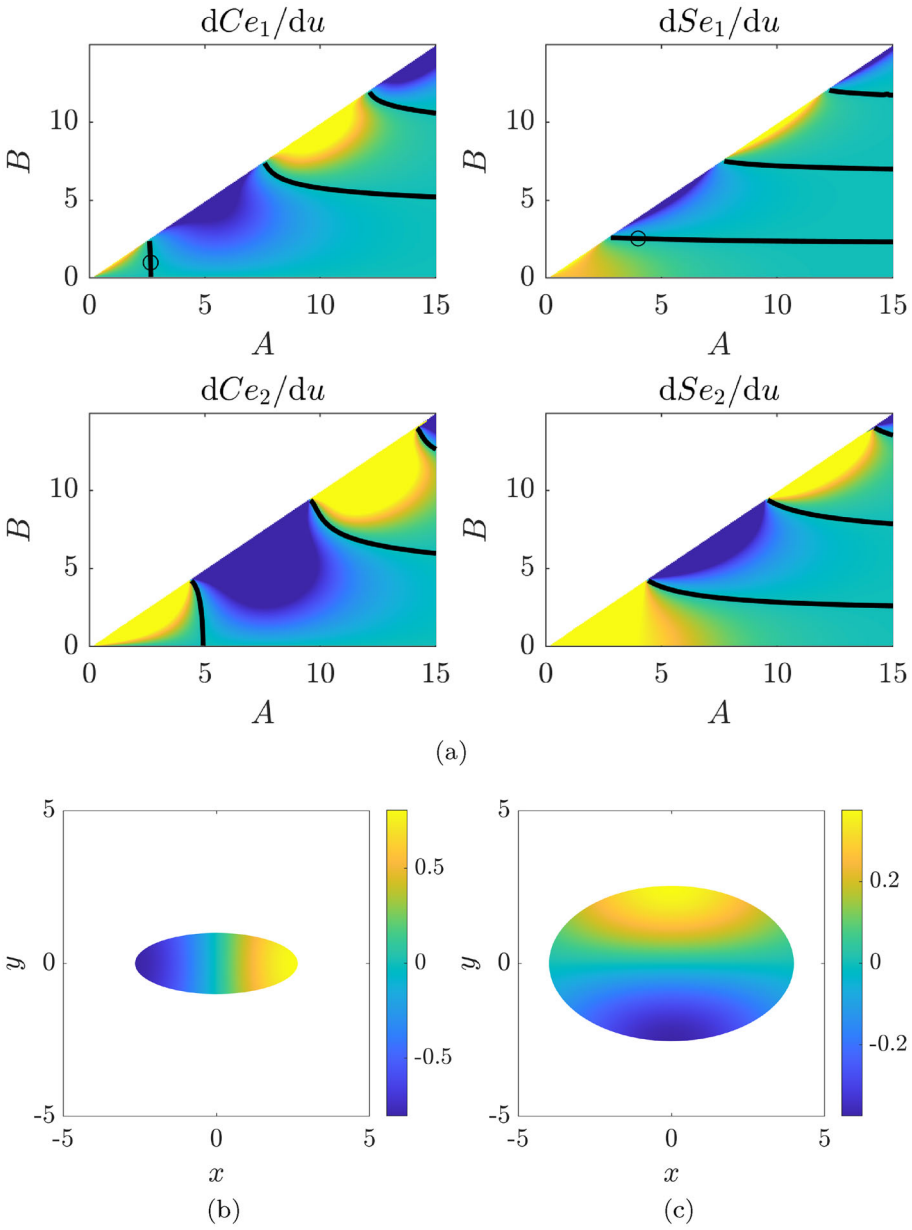

Fig. 3 **a** Plotting the values of $\mathrm{d}Ce_n/\mathrm{d}u$ and $\mathrm{d}Se_n/\mathrm{d}u$, for $n = 1$ and 2 over $(A, B) \in [0, 15] \times [0, 15]$. The colour axes are truncated at 1 (yellow) and -1 (blue). The black lines are contours where the surface is zero, *i.e.* solutions of equation (19). The black circles in the $\mathrm{d}Ce_1/\mathrm{d}u$ and $\mathrm{d}Se_1/\mathrm{d}u$ images are the parameter values used to plot (**b**, **c**), respectively. **b** Plot of $(x(u, v), y(u, v), Ce_1(u, q)ce_1(v_1, q))$, where $(A, B) = (2.66, 1)$. **c** Plot of $(x(u, v), y(u, v), Se_1(u, q)se_1(v, q))$, where $(A, B) = (4, 2.54)$

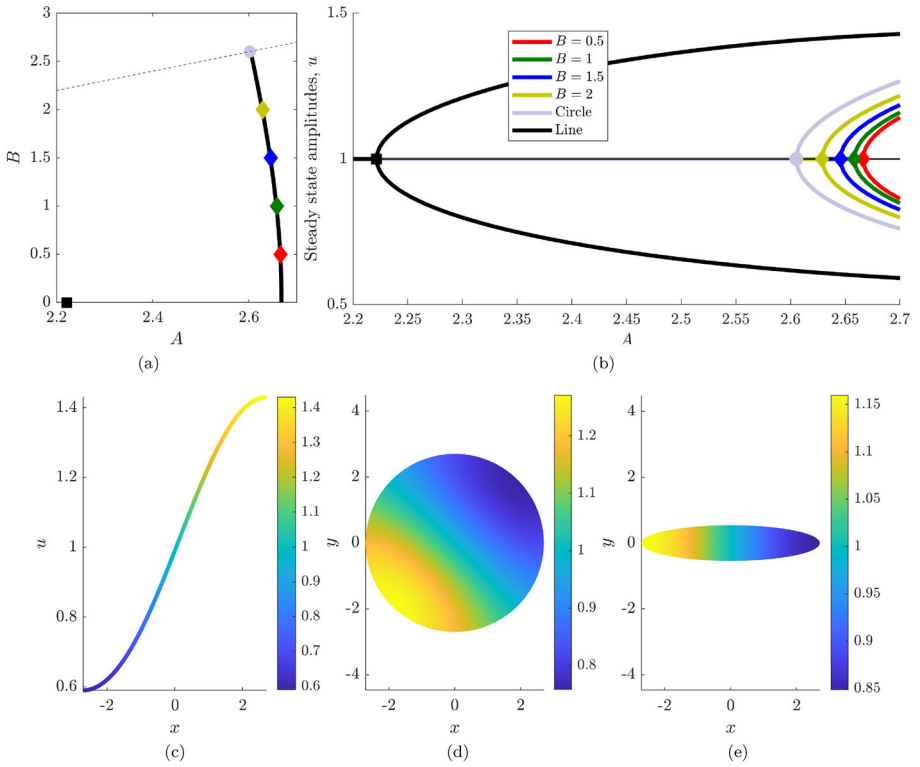

Fig. 4 **a** Zoomed image of $\mathrm{d}Ce_n/\mathrm{d}u = 0$ (thick black line) illustrating the critical radius, A_{circle}, for Turing patterns on the circle (circle marker at (2.60,2.60)) and the critical length of the one-dimensional line, A_{line}, (square marker at (2.22,0)). We also illustrate the numerically extracted values of A_{ellipse} for several values of B (diamond markers). The thin dashed line represents the line $A = B$. **b** Numerically extracted bifurcation plots of equations (21) and (22) for the line, circle and ellipses of different semi-minor axis lengths, B, see legend for details. The square, circle and coloured diamond markers illustrate the numerically derived bifurcation points and match between the (**a**, **b**) figures. Figures (**c**–**e**) illustrate the Turing pattern of ϕ formed by solving equations (21) and (22) on a line, circle and ellipse with $A = 2.7$, respectively. For the ellipse $B = 0.5$. The maximum and minimum of the colour bars match the maximum and minimum of ϕ on the, respective, domains

are seen as thick solid lines in Fig. 4b, where we observe the standard pitchfork shape of the patterned states bifurcating smoothly from the homogeneous solution.

We observe in Fig. 4b that as predicted $A_{\text{line}} < A_{\text{circle}} < A_{\text{ellipse}}(2) < A_{\text{ellipse}}(1.5) < A_{\text{ellipse}}(1) < A_{\text{ellipse}}(0.5)$. Moreover, the numerically derived critical lengths match their theoretical values as illustrated by the square, circular and diamond markers in Fig. 4a, b. Critically, the diamond markers lie on the black curve of Fig. 4a meaning that the bifurcation points, as found numerically by `pde2path`, match the solutions of $\mathrm{d}Ce_1/\,\mathrm{d}u = 0$.

The bifurcation diagrams in Fig. 4b also suggest a systematic ordering of pattern amplitudes on domains of equal width. The peak-to-trough range is largest on the one-dimensional line, smaller on the circle, and smallest on the ellipse. This ordering is confirmed by the solution visualisations in Fig. 4c–e, where the colour bars match the maximum and minimum values of ϕ on each domain.

Conclusions

For a pattern to form Turing systems require that the geometry they are simulated on be large enough to support a symmetry-breaking bifurcation. We have demonstrated that when simulating a Turing pattern on an ellipse, the patterning bifurcation properties of the ellipse tend to the bifurcation properties on a circle as the aspect ratio of the ellipse approaches unity. However, as the height of the ellipse is reduced, the bifurcation properties of the thin ellipse do not tend to those of the one-dimensional line. This result can be compared to that of a rectangular domain, where the bifurcation structure on a thin rectangle tends to a one-dimensional line. We have shown that this is because in the case of the ellipse, radial and angular aspects of the elliptic patterning modes (see Eqs. (14) and (15)) are intrinsically coupled, whereas the patterning modes decouple in the Cartesian directions on the rectangle, meaning that the one-dimensional limits of the ellipse and square are different.

Moreover, even if the critical lengths of the one-dimensional limits of the square and ellipse are different, we may have expected the bifurcation width of the ellipse, $A_{\text{ellipse}}(B)$, to lie somewhere between the bifurcation widths of the line and the circle since its geometry interpolates between the two shapes. However, we have also shown that the critical semi-major axis width of the ellipse is actually larger than the circle's critical radius for semi-minor axis lengths smaller than the circle's critical patterning radius, namely, $A_{\text{circle}} < A_{\text{ellipse}}(B)$ for all $B < A_{\text{circle}}$.

These results have implications that need to be considered if the theory of Turing patterns is to be applied to physical geometries. For example, no biological or physical domain is truly one-dimensional. Thus, as we have seen here, we must be careful to extract the correct geometry; otherwise, although the patterns will form, they will require larger shapes than we might expect. This observation is particularly relevant in morphogenesis, where tissues and organ structures often approximate elongated domains rather than perfect circles or rectangles [11, 33]. Our results indicate that while approximating thin domains as one-dimensional is convenient, care must be taken to correctly interpret the role of curvature and aspect ratio in governing pattern formation.

Similarly, in materials science and soft matter physics, self-assembled nanostructures and reaction-diffusion systems often form in constrained geometries [12]. Our findings could guide how to engineer structures to optimise stability and predict bifurcation thresholds [6].

Of course, no physical object is two-dimensional either. Future work should explore how these findings extend to three-dimensional analogues, such as transitions from an ellipsoid to a cylinder, as well as how boundary conditions impact bifurcation structures [5]. Additionally, experimental validation using chemical, or physical, Turing systems could be used to verify the physical limits to which ellipses tend, rather than just the theoretical ones. These considerations will enhance our understanding of how domain geometry influences pattern formation in both theoretical and applied contexts.

Numerical Codes

All numerical codes and plotted data can be found at https://github.com/ThomasEWoolley/Turing_ellipse/.

Author Contributions T.E.W. conceived and designed the study, carried out the mathematical analysis, performed all numerical simulations, prepared all figures, wrote the manuscript, and reviewed and approved the final version.

Funding This work received no funding.

Data Availability No datasets were generated or analysed during the current study.

Declarations

Conflict of Interest The authors declare no competing interests.

References

1. Turing, A.M.: The chemical basis of morphogenesis. Phil. Trans. R. Soc. Lond. B **237**, 37–72 (1952)
2. Kondo, S., Miura, T.: Reaction-diffusion model as a framework for understanding biological pattern formation. Science **329**(5999), 1616–1620 (2010)
3. Murray, J.D.: Mathematical Biology II: Spatial Models and Biomedical Applications, vol. 2, 3rd edn. Springer-Verlag (2003)
4. Woolley, T.E.: Pattern formation on regular polygons and circles. J. Nonlinear Sci. **35**(1), 1–44 (2025)
5. Woolley, T.E.: Boundary conditions cause different generic bifurcation structures in Turing systems. Bull. Math. Biol. **84**(9), 1–38 (2022)
6. Woolley, T.E., Krause, A.L., Gaffney, E.A.: Bespoke turing systems. Bull. Math. Biol. **83**(5), 1–32 (2021)
7. Bozzini, B., Gambino, G., Lacitignola, D., Lupo, S., Sammartino, M., Sgura, I.: Weakly nonlinear analysis of Turing patterns in a morphochemical model for metal growth. Comput. Math. Appl. **70**(8), 1948–1969 (2015)
8. Dutt, A.K.: Amplitude equation for a diffusion-reaction system: the reversible Sel'kov model. AIP Adv. **2**(4), 042125 (2012)
9. Sadier, A., Twarogowska, M., Steklikova, K., Hayden, L., Lambert, A., Schneider, P., Laudet, V., Hovorakova, M., Calvez, V., Pantalacci, S.: Modeling Edar expression reveals the hidden dynamics of tooth signaling center patterning. PLoS Biol. **17**(2), e3000064 (2019)
10. Hale, J.K., Raugel, G.: A reaction-diffusion equation on a thin L-shaped domain. Proc. R. Soc. Edinb., Sect. A, Math. **125**(2), 283–327 (1995)
11. Seirin-Lee, S.: Role of domain in pattern formation. Dev. Growth Differ. **59**(5), 396–404 (2017)
12. Shevchenko, V.Y., Makogon, A.I., Sychov, M.M., Nosonovsky, M., Skorb, E.V.: Reaction-diffusion pathways for a programmable nanoscale texture of the diamond-SiC composite. Langmuir **38**(49), 15220–15225 (2022)
13. Tanaka, M., Song, Y., Nomura, T.: Fabric soft pneumatic actuators with programmable turing pattern textures. Sci. Rep. **14**(1), 19175 (2024)
14. Korn, G.A., Korn, T.M.: Mathematical Handbook for Scientists and Engineers, vol. 25. McGraw-Hill, New York (1968)
15. Troesch, B.A., Troesch, H.R.: Eigenfrequencies of an elliptic membrane. Math. Comput. **27**(124), 755–765 (1973)
16. Arfken, G.B., Weber, H.J.: Mathematical Methods for Physicists. Elsevier Academic Press (2011)
17. Karbowiak, A.E.: The elliptic surface wave. Brit. J. Appl. Phys. **5**(9), 328 (1954)
18. Wu, Y., Shivakumar, P.N.: Eigenvalues of the Laplacian on an elliptic domain. Comput. Math. Appl. **55**(6), 1129–1136 (2008)
19. Chen, G., Morris, P.J., Zhou, J.: Visualization of special eigenmode shapes of a vibrating elliptical membrane. SIAM Rev. **36**(3), 453–469 (1994)
20. Woolley, T.E., Baker, R.E., Maini, P.K.: The Turing Guide, Chapter 35: Turing's Theory of Morphogenesis. Oxford Univ. Press (2017)

21. Maini, P.K., Woolley, T.E.: The Turing Model for Biological Pattern Formation, pp. 189–204. Springer (2019)
22. Hettich, R., Haaren, E., Ries, M., Still, G.: Accurate numerical approximations of eigenfrequencies and eigenfunctions of elliptic membranes. ZAMM-J. Appl. Math. Mech./Zeitschrift für Angewandte Mathematik und Mechanik **67**(12), 589–597 (1987)
23. Mathieu, É.: Mémoire sur le mouvement vibratoire d'une membrane de forme elliptique. Journal de mathématiques pures et appliquées **13**, 137–203 (1868)
24. McLachlan, N.W.: Theory and Application of Mathieu Functions. Clarendon Press (1951)
25. Arscott, F.M., Sneddon, I.N., Stark, M., Ulam, S.: Periodic Differential Equations: An Introduction to Mathieu, Lamé, and Allied Functions. Pergamon (2014)
26. Woolley, T.E., Baker, R.E., Maini, P.K.: Turing's theory of morphogenesis: where we started, where we are and where we want to go. The Incomputable: Journeys Beyond the Turing Barrier, pages 219–235, (2017)
27. Maini, P.K., Woolley, T.E., Baker, R.E., Gaffney, E.A., Lee, S.S.: Turing's model for biological pattern formation and the robustness problem. Interface Focus **2**(4), 487–496 (2012)
28. Frenkel, D., Portugal, R.: Algebraic methods to compute Mathieu functions. J. Phys. A: Math. Gen. **34**(17), 3541 (2001)
29. Whittaker, E.T., Watson, G.N.: A Course of Modern Analysis. University Press (1963)
30. Schnakenberg, J.: Simple chemical reaction systems with limit cycle behaviour. J. Theor. Biol. **81**(3), 389–400 (1979)
31. Uecker, H.: Continuation and Bifurcation in Nonlinear PDEs-Algorithms, Applications, and Experiments. Jahresber. Dtsch. Math.-Ver., pages 1–38, (2021)
32. Uecker, H.: Numerical Continuation and Bifurcation in Nonlinear PDEs. SIAM (2021)
33. Irvine, K.D., Shraiman, B.I.: Mechanical control of growth: ideas, facts and challenges. Development **144**(23), 4238–4248 (2017)